ACS APPLIED MATERIALS & INTERFACES

Research Article

www.acsami.org

Ternary Bulk Heterojunction Solar Cells: Addition of Soluble NIR Dyes for Photocurrent Generation beyond 800 nm

Bogyu Lim,[†,§,∥] Jason T. Bloking,[†,∥] Andrew Ponec,[†] Michael D. McGehee,[†] and Alan Sellinger*[,†,‡]

[†]Department of Materials Science and Engineering, Geballe Laboratory for Advanced Materials, Stanford University, 476 Lomita Mall, Stanford, California 94305, United States

[‡]Department of Chemistry and Geochemistry, Colorado School of Mines, 1012 14th Street, Golden, Colorado 80401, United States

Supporting Information

ABSTRACT: The incorporation of a *tert*-butyl-functionalized silicon 2,3-naphthalocyanine bis(trihexylsilyloxide) dye molecule as a third component in a ternary blend bulk heterojunction (BHJ) organic solar cell containing P3HT (donor) and $PC_{60}BM$ (acceptor) results in increased NIR absorption. This absorption yields an increase of up to 40% in the short-circuit current and up to 19% in the power conversion efficiency (PCE) in photovoltaic devices. Two-dimensional grazing incidence wide-angle X-ray scattering (2-D GIWAXS) experiments show that compared to the unfunctionalized dye the *tert*-butyl functionalization enables an increase in the volume fraction of the dye molecule that can be incorporated before the device performance decreases. Quantum efficiency and absorption spectra also indicate that, at dye concentrations above about 8 wt %, there is an approximately 30 nm red shift in the main silicon naphthalocyanine absorption peak, allowing further dye addition to contribute to added photocurrent. This peak shift is not observed in blends with unfunctionalized dye molecules, however. This simple approach of using ternary blends may be generally applicable for use in other unoptimized BHJ systems towards increasing PCEs beyond current levels. Furthermore, this may offer a new approach towards OPVs that absorb NIR photons without having to design, synthesize, and purify complicated donor−acceptor polymers.

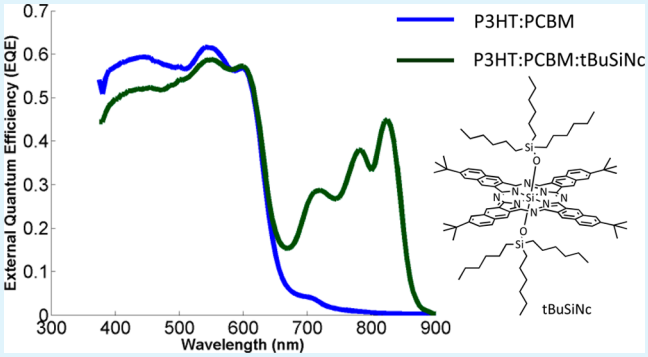

KEYWORDS: *solar cells, organic electronics, conjugated polymers, photovoltaic devices*

INTRODUCTION

Bulk heterojunction (BHJ) organic solar cells from blends of two conjugated organic polymers or small molecules have attracted considerable attention over the past two decades due to their potential for solar energy generation with low manufacturing cost, light weight, flexibility, and simple large-scale fabrication.[1−6] Among the blended materials systems used in BHJ devices, the one comprising poly(3-hexylthiophene), P3HT, as the electron donor and [6,6]-phenyl C_{60} butyric acid methyl ester, $PC_{60}BM$, as the electron acceptor is the most extensively studied.[7−11] However, the power conversion efficiency of most P3HT:$PC_{60}BM$ bulk heterojunction solar cells remains between 3.8% and 4%.[7,12,13] This is due in part to the bandgap (E_g) of P3HT (the dominant absorber in the active layer) having a value of 1.9 eV, so only photons in the green and blue parts of the spectrum with wavelengths below 650 nm are absorbed, leading to a typical short-circuit current (J_{SC}) of 8−12 mA/cm^2.[7] In addition to the lower J_{SC}, there are large energetic offsets between the HOMO and LUMO levels of the P3HT and $PC_{60}BM$, resulting in an open-circuit voltage (V_{OC}) that is about 1.1 V lower than the value of E_g/q of 1.7 V for $PC_{60}BM$. This energy loss is significantly more than the 0.7−0.85 V lost in some of the most efficient BHJ organic solar cells.[14−24]

To increase the power conversion efficiency of solar cells, new donor polymers have been developed that absorb light either in the near-IR region (increasing J_{SC})[17,25−28] or with different energy levels to reduce the energetic offsets between donor and acceptor (increasing V_{OC}).[14,18,19,21−23,29−32] These developments have led to organic photovoltaic devices achieving published efficiencies of 9.35%[24] in academic research laboratories and of greater than 10%[33] in industrial research laboratories. In addition to these efficient polymer-based donor molecules, solar cells using small organic molecules as donors have also reached 9% efficiencies.[34,35] Still, absorption of the solar spectrum beyond 750 nm in some of these devices remains an opportunity for the enhancement of short-circuit current.

To improve light harvesting beyond 700 nm in BHJ organic solar cells, incorporation of additional organic components,[36] such as dye molecules[37−43] or additional polymers,[44−49] has

Received: February 2, 2014
Accepted: April 22, 2014
Published: April 23, 2014

been reported. Dyes with strong absorption in the near-IR region can easily be incorporated into BHJ films through blending of the dye molecule in the donor−acceptor solution. However, despite this relatively simple method of increasing light harvesting, very few reports of improved efficiencies due to dye incorporation are found.[50−53] In fact, due to mismatched energy levels or the disruption of the optimized bulk heterojunction morphology, some ternary blend BHJ solar cells see a reduction in efficiency compared to their binary blend counterparts. In other recent reports, ternary blend solar cells between $PC_{60}BM$ and two donor polymers[54] and between P3HT and two different fullerene derivatives[55−57] demonstrated a V_{OC} that changes linearly with composition between the two binary blend end points. This has been correlated with an equivalent variation in the charge-transfer state energy (E_{CT}) and provides additional insight into the fundamental workings of organic solar cells as well as an opportunity to fine-tune the V_{OC} to optimize efficiency.[58]

Recently, Honda and co-workers reported increased light harvesting using silicon(IV) phthalocyanine bis(trihexylsilyloxide) (SiPc) and silicon 2,3-naphthalocyanine bis(trihexylsilyloxide) (SiNc).[39,59−61] The SiPc and SiNc molecules have strong absorption bands that do not overlap with the absorption spectra of either P3HT or $PC_{60}BM$, providing complementary absorption profiles. In addition, the presence of the bulky trihexylsilyloxide side groups reduces the tendency of the molecules to aggregate compared to other phthalocyanines and naphthalocyanines.[39] The incorporation of SiPc resulted in a 20% increase in power conversion efficiency over the control devices as a result of increased J_{SC}.[60]

In this paper, we report a significant improvement to the J_{SC} in P3HT:$PC_{60}BM$ bulk heterojunction solar cells due to an increase in the near-IR light-harvesting capability using *tert*-butyl-functionalized silicon 2,3-naphthalocyanine bis(trihexylsilyloxide) (*t*-butyl SiNc, Figure 1a) as the third component in a ternary blend. The short-circuit current increases steadily with the addition of up to 20 wt % *t*-butyl SiNc, a dye loading significantly higher than what previous tests have shown to be optimal. We demonstrate that the reason for the increased optimal dye loading concentration is that the addition of the *t*-butyl functional groups allows a higher degree of compatibility between the dye molecule and the nanoscale morphology of the P3HT:$PC_{60}BM$ bulk heterojunction as well as a lower degree of aggregation. Interestingly, a bathochromic shift in the *t*-butyl SiNc absorption and photocurrent spectra is seen upon thermal annealing of ternary blend films with dye loadings of higher than approximately 8 wt %. This shift is speculated to be the result of the formation of a new morphological state of the dye molecules when blended, perhaps as a dimer or in an aggregated phase, which allows the effective incorporation of greater amounts of *t*-butyl SiNc compared to unfunctionalized SiNc. This additional dye incorporation enables the enhancement of J_{SC} in P3HT:*t*-butyl SiNc:$PC_{60}BM$ ternary blend organic solar cells by as much as 40% (32% average) and achieves a PCE of up to 4.9% (4.5% average) in devices.

EXPERIMENTAL DETAILS

Materials. Regioregular P3HT was purchased from Rieke Metals, Inc. (#4002-E, M_n = 22 700 g/mol, M_w = 50 000 g/mol, PDI = 2.20 (GPC), regioregularity 93%) and used as received without further purification. Where specified in the manuscript, regioregular P3HT from BASF (Sepiolid P200, M_n = 13 400 g/mol, M_w = 21 800 g/mol, PDI = 1.63 (GPC), regioregularity ≥95% and ≤10 ppm of Fe, Pd, and Sn, 12 ppm of Zn, and 28 ppm of Ni) was used. $PC_{60}BM$ was purchased from Nano-C and used without further purification. Unfunctionalized silicon naphthalocyanine (SiNc) was purchased from Sigma-Aldrich and used without further purification. 6-*tert*-Butyl-2,3-dihydro-1,3-diimino-1*H*-benz[*f*]isoindole (**1**) was prepared according to procedures in the literature.[62]

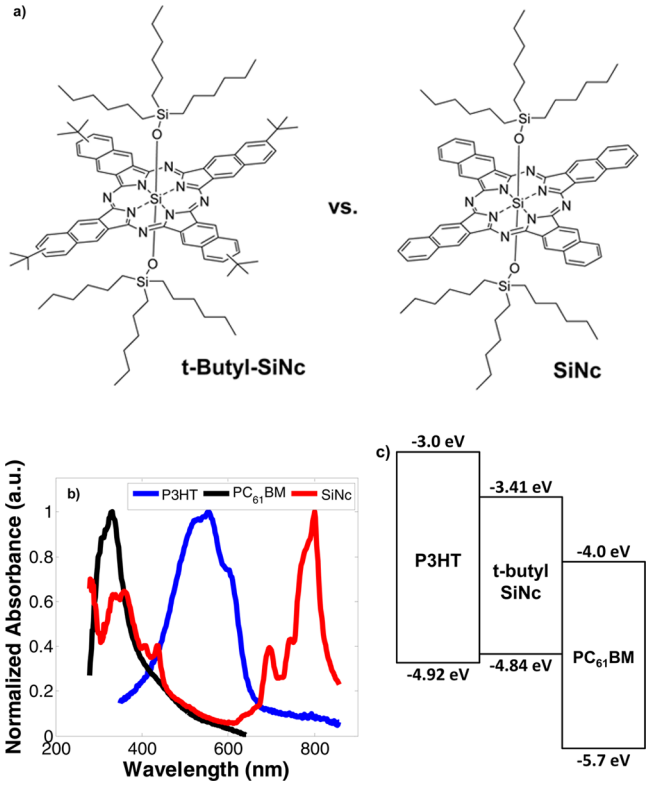

Figure 1. (a) Chemical structures of *tert*-butyl silicon naphthalocyanine (left) and unfunctionalized silicon naphthalocyanine (right). (b) Normalized thin-film absorption spectra of $PC_{60}BM$, P3HT, and *t*-butyl SiNc dye. (c) Energy level diagram for the P3HT:*t*-butyl SiNc:$PC_{60}BM$ ternary blend system.

Synthesis of Compound ***3***. Tetrachlorosilane (1.20 mL, 10.5 mmol) was added to a suspension of 6-*tert*-butyl-2,3-dihydro-1,3-diimino-1*H*-benz[*f*]isoindole (**1**) (1.88 g, 7.5 mmol) in 30 mL of quinoline at room temperature under nitrogen. The mixture was heated to 210 °C and stirred for 2 h. After cooling slowly, 70 mL of methanol was added, and the resulting mixture was stirred overnight. The reddish-brown mixture was filtered and washed with methanol and then dried (1.26 g) before use for subsequent reaction without further purification. The green solid (compound **2**) was added to concentrated H_2SO_4 (20 mL) and stirred for 2 h. The mixture was poured onto 20 g of ice water and then vigorously stirred overnight. The precipitate formed was filtered and washed with water and then methanol. The resulting green solid (1.22 g) was refluxed in a 1:1 mixture of pyridine and 25% NH_4OH (20 mL) for 10 h. After cooling to room temperature, the insoluble material was filtered, washed with water and ethanol, and then dried to give a crude dark green solid (compound **3**, 1.06 g), which was used for subsequent reactions without further purification.

Synthesis of Compound tert-Butyl SiNc.[63] Chlorotrihexylsilane (1.83 mL, 5 mmol) was added to a suspension of compound **3** (1.04 g, 1.05 mmol) in dry pyridine. The mixture was stirred for 2 h under reflux. After cooling, the reaction mixture was poured into 250 mL of a 1:1 mixture of ethanol and water before stirring overnight. The precipitated green solid was filtered and washed with water and then ethanol before purification by column chromatography with hexane to obtain a dark-green powder as product. Yield: 0.25 g (15%). ^{1}H NMR

dx.doi.org/10.1021/am5007172 | ACS Appl. Mater. Interfaces 2014, 6, 6905−6913

(see Figure S1, Supporting Information, 400 MHz, $CDCl_3$, δ): 10.07 (d, 8H, J = 13.96 Hz), 8.60 (d, J = 9.15 Hz, 8H), 8.01 (d, J = 9.15 Hz, 4H), 1.65 (s, 36H), 0.63 (m, 12H), 0.38 (t, 18H, J = 14.72 Hz), 0.19 (m, 12H), 0.07 (m, 12H), −1.01 (m, 12H), −2.06 (m, 12H). ^{13}C NMR (see Figure S2, Supporting Information, 500 MHz, $CDCl_3$, δ): 150.25, 149.23, 134.87, 133.48, 133.09, 132.98, 129.89, 126.62, 125.16, 123.51, 122.94, 35.38, 33.61, 33.45, 31.81, 31.60, 31.42, 23.40, 23.34, 22.87, 22.72, 22.07, 14.41, 14.14, 13.90, 13.65, 13.48. MALDI-TOF (see Figure S3, Supporting Information) m/z: $[M]^+$ calcd for *tert*-butyl SiNc, 1564.0; found, 1564.3.

Materials Characterization. Materials were characterized by ^{1}H NMR spectroscopy (Varian, 400 MHz) and ^{13}C NMR spectroscopy (Inova 500 MHz). Absorption and photoluminescence spectra were measured using a Cary 6000i UV/Vis spectrophotometer and Horiba Jobin-Yvon Spex Fluorolog-3 fluorimeter, respectively. Molecular weight was determined with a Bruker UltrafleXtreme MALDI/TOF-TOF mass spectrometer. Cyclic voltammetry (CV) was conducted using a VMP3 (Bio-Logic) potentiostat in a dichloromethane solution with 0.1 M tetrabutylammonium hexafluorophosphate ($TBAPF_6$) as supporting electrolyte, glassy carbon as the working electrode, Pt wire as the counter electrode, and Ag wire as the reference electrode at a scan rate of 50 mV s^{-1}.

Device Preparation. A 1:1 (by weight) co-solution of poly(3-hexylthiophene) (P3HT, Rieke Metals, 4002-E-grade or Sepiolid (P200, BASF) and [6,6]-phenyl C_{60} butyric acid methyl ester ($PC_{60}BM$, Nano-C) in 1,2-dichlorobenzene (Aldrich) was prepared at a total solid concentration of 50 mg mL^{-1}. Solutions of the *t*-butyl SiNc and unfunctionalized SiNc in 1,2-dichlorobenzene were also prepared at a concentration of 50 mg mL^{-1}. These solutions were left overnight to stir on a hot plate at a temperature of 115 °C to ensure complete dissolution of the compounds in the solvent. The *t*-butyl SiNc and unfunctionalized SiNc solutions were then mixed separately with the P3HT:$PC_{60}BM$ solution in controlled amounts to vary the final amount of dye in the ternary blend film. These mixed solutions were allowed to spin on a hot plate for at least 2 h at 65 °C to ensure the solutions were fully mixed before deposition.

Bulk heterojunction solar cells were prepared as stacks of indium tin oxide (ITO, 110 nm)/PEDOT:PSS (25 nm)/P3HT:$PC_{60}BM$:*t*-butyl SiNc (ca. 220 nm)/Ca (7 nm)/Al (150 nm). Patterned ITO-coated glass substrates (Xin Yan Technologies, 15 Ω sq^{-1}) were scrubbed in a detergent solution (Extran 300, 10× dilution), followed by a 15 min sonication process in the same detergent solution. Substrates were then rinsed in flowing DI water for 5 min, followed by additional 15 min sonication steps in acetone and isopropanol successively. Substrates were then blown dry with a pressurized dry nitrogen stream before undergoing UV-ozone treatment for 15 min. These substrates were then coated with approximately 25 nm of poly(3,4-ethylenedioxythiophene):poly(styrenesulfonate) (PEDOT:PSS, Clevios P VP AI 4083) via spin-coating at 4000 rpm for 30 s. Substrates were then dried in air on a hot plate at 140 °C for 10 min before transferring into a dry, nitrogen-filled glove box (<5 ppm of O_2) for further processing. All steps prior to transferring into the nitrogen glove box were performed inside a laminar flow hood to minimize the adsorption of dust particles during processing. Once inside the glove box, the ternary blend active layer was deposited via spin-coating at 900 rpm for 45 s directly from the solution at 65 °C. After spinning, samples were quickly placed in a covered petri dish to allow the active layer to dry slowly overnight. After drying, the samples were thermally annealed (if desired) inside the glove box at 110 °C for 10 min before sequential thermal evaporation of Ca (7 nm) and Al (150 nm) in an Angstrom Engineering thermal evaporator system at a pressure below 1 × 10^{-6} Torr.

Device Characterization. All device characterization was performed inside a nitrogen atmosphere with the sample having never been exposed to oxygen prior to testing. Current density (J)−voltage (V) curves of completed solar cells were collected using a simulated AM1.5G solar spectrum from a Xe arc lamp using an NREL-calibrated KG5-filtered Hamamatsu photodiode to reduce spectral mismatch during calibration. External quantum efficiency (EQE) spectra were collected using a monochromatic light source and were calibrated to a NIST-traceable Si photodiode. Two-dimensional grazing incidence wide-angle X-ray scattering (2-D GIWAXS) experiments were performed at the Stanford Synchrotron Radiation Lightsource (SSRL) at beamline 11-3 using 12.7 keV X-ray radiation and calibrated using a LaB_6 crystal.

RESULTS AND DISCUSSION

Figure 1a depicts the molecular structures of *t*-butyl SiNc and unfunctionalized SiNc. The *t*-butyl-functionalized SiNc was synthesized as shown in Scheme S1 (see Supporting Information) in a manner similar to the procedures found in our previous report.[63] The key feature of this new dye is the incorporation of four bulky *tert*-butyl substituents to the periphery of the molecule, which improves solubility in common organic solvents and reduces the likelihood of large-scale aggregation due to weaker intermolecular interactions between the conjugated naphthalocyanine cores of adjacent molecules.

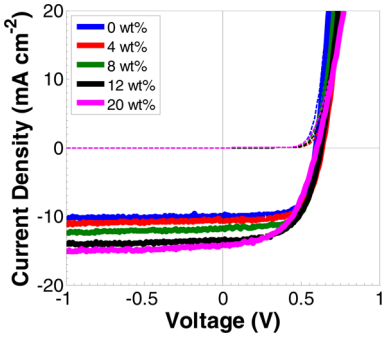

Figure 2. Current density vs voltage curves for Rieke P3HT:$PC_{60}BM$ BHJ devices with increasing amounts of *t*-butyl SiNc dye addition.

Table 1. P3HT:$PC_{60}BM$ Device Performance with Increasing *t*-Butyl SiNc Dye Concentration[a]

dye conc. (wt %)	J_{SC} (mA cm^{-2})	V_{OC} (V)	FF (%)	PCE (%)
0	9.4 (10.1)	0.60 (0.62)	67 (71)	3.80 (4.12)
2	10.1 (10.5)	0.62 (0.63)	65 (68)	4.11 (4.43)
4	10.1 (10.7)	0.63 (0.64)	65 (68)	4.18 (4.42)
6	10.7 (11.1)	0.62 (0.64)	64 (69)	4.27 (4.56)
8	11.4 (12.1)	0.62 (0.64)	63 (68)	4.46 (4.92)
10	11.6 (12.5)	0.61 (0.63)	62 (68)	4.46 (4.80)
12	12.4 (13.7)	0.62 (0.62)	57 (61)	4.36 (4.91)
15	11.2 (14.0)	0.61 (0.62)	59 (64)	3.97 (4.69)
20	11.1 (14.2)	0.60 (0.62)	58 (64)	3.92 (4.93)

[a]Note: Performance values are averages with champion cell values in parentheses.

The absorption characteristics and oxidation/reduction properties of the *t*-butyl and unfunctionalized SiNc molecules were measured by UV-vis spectroscopy (see Figure S4, Supporting Information) and cyclic voltammetry (see Figure S5, Supporting Information). The introduction of the *t*-butyl groups does not significantly affect either the redox potentials or the absorption characteristics of the molecule. The *t*-butyl SiNc exhibits a high absorption coefficient in solution (ε = 4.09 × 10^5 M^{-1} cm^{-1} at 776 nm) that is equivalent to the maximum absorption coefficient in solution of the unfunctionalized SiNc (ε = 4.15 × 10^5 M^{-1} cm^{-1} at 773 nm). In the solid state, the optical absorption spectrum of the *t*-butyl SiNc exhibits a strong Q-band absorption at approximately 800 nm. The

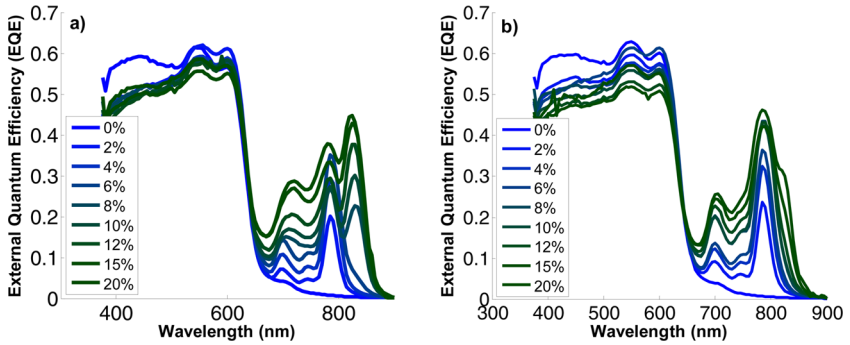

Figure 3. EQE spectra of (a) thermally annealed and (b) unannealed P3HT:$PC_{60}BM$:*t*-butyl SiNc devices vs *t*-butyl SiNc concentration.

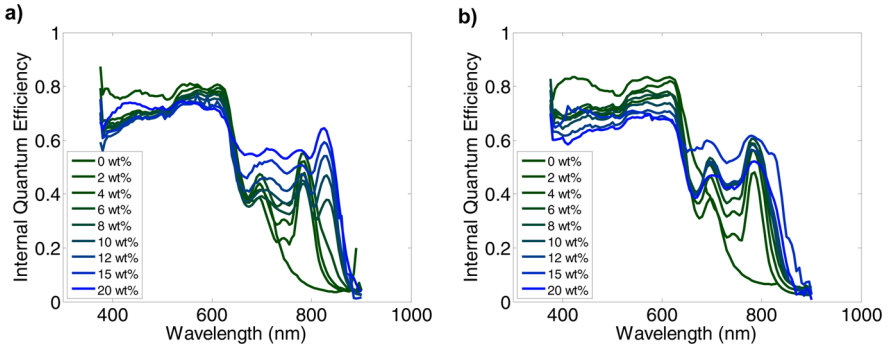

Figure 4. Internal quantum efficiency (IQE) spectra for (a) thermally annealed and (b) unannealed P3HT:$PC_{60}BM$:*t*-butyl SiNc devices vs *t*-butyl SiNc concentration.

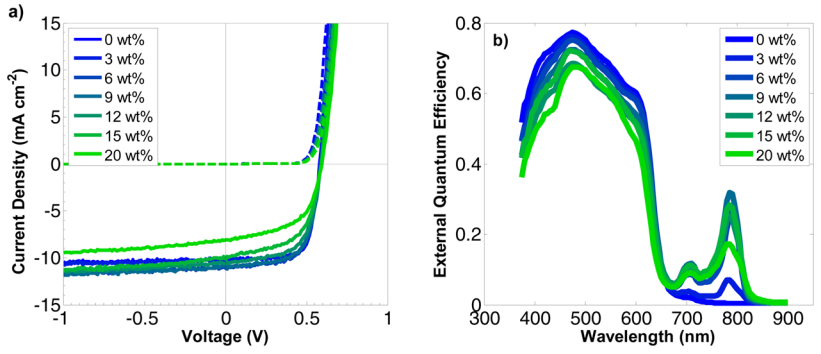

Figure 5. (a) *J*–*V* curves and (b) EQE spectra of P3HT:$PC_{60}BM$ devices with increasing amounts of unfunctionalized SiNc concentration. Cells were thermally annealed at 110 °C for 10 min.

Table 2. P3HT:$PC_{60}BM$ Device Performance with Increasing Unfunctionalized SiNc Dye Concentration

Dye Conc. (wt %)	J_{SC} (mA cm^{-2})	V_{OC} (V)	FF (%)	PCE (%)
0	9.4 (10.1)	0.60 (0.62)	67 (71)	3.80 (4.12)
3	10.0 (10.1)	0.59 (0.59)	72 (72)	4.22 (4.26)
6	10.9 (10.9)	0.59 (0.59)	67 (68)	4.26 (4.35)
9	10.6 (10.9)	0.59 (0.59)	66 (65)	4.12 (4.18)
12	10.2 (10.6)	0.58 (0.59)	57 (63)	3.37 (3.94)
15	9.8 (9.6)	0.59 (0.59)	58 (61)	3.34 (3.47)
20	7.8 (8.1)	0.59 (0.59)	54 (56)	2.49 (2.70)

absorption spectra of the SiNc molecules do not overlap significantly with the absorption spectra of several donor molecules (such as P3HT, see Figure 1b) used in organic solar cells, promising complementary absorption profiles and enhanced solar spectrum capture.

The HOMO and LUMO levels as measured by cyclic voltammetry (see Figure S5, Supporting Information) are −4.84 and −3.41 eV, respectively. A diagram of the energy levels in a ternary blend cell of P3HT:*t*-butyl SiNc:$PC_{60}BM$ is shown in Figure 1c demonstrating the possibility that excitons created on the *t*-butyl SiNc molecules can undergo electron transfer to the $PC_{60}BM$ or hole transfer to the P3HT. On the basis of energetic and absorption measurements, the *t*-butyl SiNc can improve the overall efficiency as a third component in a ternary blend organic solar cell.

To investigate the photovoltaic performance of P3HT:$PC_{60}BM$ devices to which *t*-butyl SiNc was added, we fabricated BHJ solar cells using a typical device stack of indium tin oxide (ITO, 110 nm)/PEDOT:PSS (25 nm)/P3HT:*t*-butyl SiNc:$PC_{60}BM$ (220 ± 20 nm)/Ca (7 nm)/Al (150 nm). The thickness of all cells was not measured, but representative cells that were measured using a profilometer at a variety of *t*-butyl concentrations consistently exhibited thicknesses of 220 ± 20

dx.doi.org/10.1021/am5007172 | ACS Appl. Mater. Interfaces 2014, 6, 6905−6913

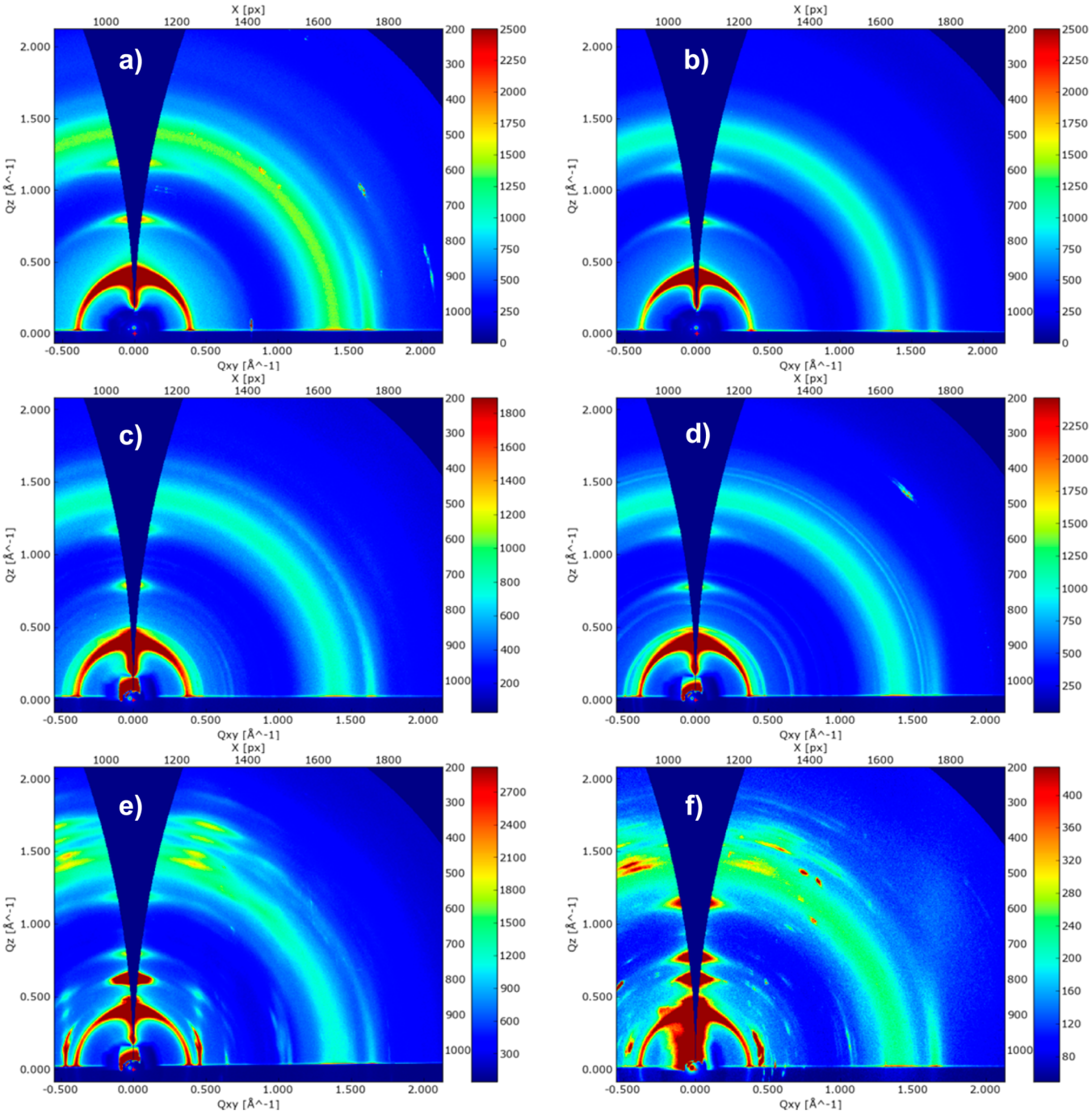

Figure 6. Two-dimensional X-ray scattering patterns for P3HT:$PC_{60}BM$ films with the following dye additions and thermal treatments: (a) no dye, unannealed; (b) no dye, annealed; (c) 20 wt % *t*-butyl SiNc, unannealed; (d) 20 wt % *t*-butyl SiNc, annealed; (e) 20 wt % unfunctionalized SiNc, unannealed; (f) 20 wt % unfunctionalized SiNc, annealed.

nm. Prior to Ca/Al cathode deposition via thermal evaporation, films were thermally annealed at 110 °C for 10 min. Figure 2 shows the *J*−*V* characteristics of devices with different *t*-butyl SiNc concentrations, and Table 1 summarizes the photovoltaic performance parameters. The reference devices without *t*-butyl SiNc exhibited average solar cell performance parameters of a V_{OC} of 0.60 V, a J_{SC} of 9.4 mA cm^{-2}, a fill factor of 67%, and a PCE of 3.80%. The performance of champion devices is included in parentheses in Table 1. The incorporation of the *t*-butyl SiNc dye improved the J_{SC} to 12.4 mA cm^{-2} at 12 wt %, an increase of 32%. The highest J_{SC} observed in any device was 14.2 mA cm^{-2} at a *t*-butyl concentration of 20 wt %. This maximum increase in J_{SC} resulted in an observed power conversion efficiency of 4.93% with a highly regioregular P3HT (Sepiolid P200 from BASF) blended with $PC_{60}BM$. It should be noted that the J_{SC} of champion devices increased linearly with dye loading up to about 20 wt % unlike previous reports with unfunctionalized SiPc or SiNc addition, which found maximum PCE values at 4.8 wt % for SiPc and 1.5 wt % for SiNc.[59] These results suggest that the *t*-butyl functionalization has a significant impact on the nature of the dye molecule incorporation, allowing for larger volume fractions of dye molecules to be incorporated before the morphology of the P3HT:$PC_{60}BM$ BHJ cell is disrupted.

dx.doi.org/10.1021/am5007172 | *ACS Appl. Mater. Interfaces* 2014, 6, 6905−6913

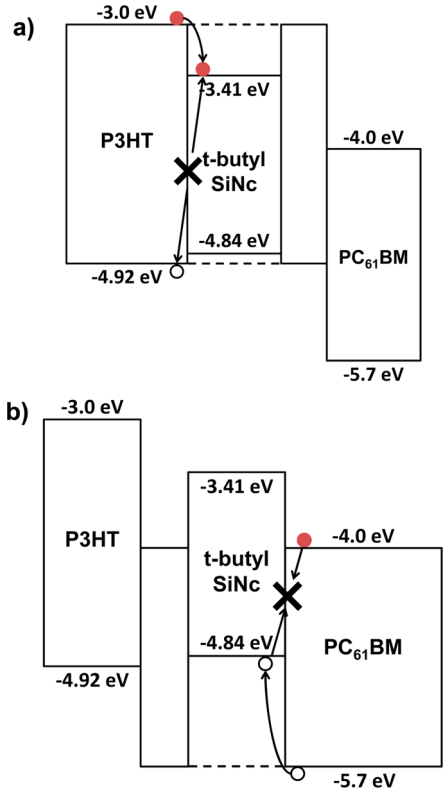

Figure 7. Energy level diagrams for ternary blend with (a) dye wholly dispersed within the P3HT phase and (b) dye wholly dispersed within the $PC_{60}BM$ phase.

The spectral breakdown of the photocurrent in the ternary blend cells is shown in the external quantum efficiency (EQE) spectra shown in Figure 3. As the concentration of the *t*-butyl SiNc is increased in the ternary blend, peaks associated with the *t*-butyl SiNc absorption in the 700−800 nm spectral range increase proportionately. These peaks are due to direct photoexcitation of the *t*-butyl SiNc. The strongest peak in the EQE spectrum at 800 nm increased to a value of 35% as the concentration of *t*-butyl SiNc was increased to 8 wt %. A decrease from about 60% to 55% was observed in the EQE spectrum between 550 and 600 nm where the P3HT absorbs most of the light and from about 57% to 49% between 400 and 500 nm where $PC_{60}BM$ is primarily absorbing. These changes could be due either to a decrease in the absorption as the volume fraction of P3HT and $PC_{60}BM$ is reduced in favor of the *t*-butyl SiNc or to a reduction in the internal quantum efficiency (IQE).

Interestingly, at dye loadings between 8 and 20 wt %, a new peak in the EQE spectrum appears at 830 nm, increasing linearly up to an EQE value of 45%. This new peak exhibits a bathochromic shift of 30 nm by the main absorption peak of the *t*-butyl SiNc at 799 nm that occurs at higher dye loadings. However, this peak at 830 nm is not visible in the absorption spectrum of the pure *t*-butyl SiNc film (see Figure 1b), suggesting that the morphological nature of the *t*-butyl SiNc molecules is different in the ternary blend film as compared to the pure film. To investigate this absorption peak further, we prepared binary blend films of both P3HT and $PC_{60}BM$ with *t*-butyl SiNc and collected their absorption spectra (see Figures S6 and S7, Supporting Information). The peak at 830 nm was not visible in either of these configurations, eliminating the possibility of the new peak being caused by a coupling reaction between the *t*-butyl SiNc and either the P3HT or $PC_{60}BM$, as has been seen in other reports on covalent links between phthalocyanine molecules and carbon nanotubes.[64] We also collected EQE spectra of P3HT:*t*-butyl SiNc:$PC_{60}BM$ without thermal annealing to determine the role of temperature in the formation of this additional peak. Figure 3b demonstrates that in the absence of a thermal annealing step the new peak does not appear, except for a shoulder appearing in the 20 wt % *t*-butyl SiNc device. The second peak at 830 nm was also seen in the device absorption spectra of blends with a different donor material, poly(di(2-ethylhexyloxy)benzo[1,2-b:4,5-b']-dithiophene-*co*-octylthieno[3,4-*c*]pyrrole-4,6-dione) (PBDTTPD, see Figure S8, Supporting Information), suggesting that the specific donor polymer is not critical to its appearance. Surprisingly, however, the peak did not appear in the device EQE (see Figure S9, Supporting Information). This suggests that the cause of the *t*-butyl SiNc absorption shift results in a change such that photocurrent can no longer be generated. This could be due to a change in the energetics of the molecule preventing efficient hole (electron) transfer to the PBDTTPD ($PC_{60}BM$). Overall, the second absorption peak at 830 nm is only found in ternary blends that have been thermally annealed at *t*-butyl SiNc concentrations greater than about 8 wt %.

To verify that the increased J_{SC} seen in the $J-V$ curves is real and not an artifact due to poor spectral mismatch between the solar spectrum and our solar simulator in the 800 nm region, we integrated the relevant EQE spectra in Figure 3 to determine the short-circuit photocurrent. While the integrated J_{SC} values are between 4% and 16% lower than those measured in the solar simulator, there remains a smooth, monotonic increase in the integrated J_{SC} with increasing dye concentration for the thermally annealed samples in Figure 3a and a decrease in the integrated J_{SC} at high dye loadings in the unannealed samples in Figure 3b (see Figures S10 and S11, Supporting Information).

To evaluate the efficacy of the exciton splitting and charge separation processes, we calculated the internal quantum efficiency (IQE) spectra from the measured EQE spectra and active layer absorption in each device. The active layer absorption was determined by measuring the total device absorption using an integrating sphere and subtracting off the absorption in the ITO, PEDOT:PSS, and Ca/Al layers determined through the use of a transfer matrix calculation according to the methods of Burkhard et al.[65] This allows a more accurate determination of the true active layer absorption and hence the internal quantum efficiency.

The IQE spectra are shown in Figures 4a and 4b for the annealed and unannealed devices, respectively. It is clear that the IQE of the P3HT:$PC_{60}BM$ absorption averages between about 60% and 80%, which is typical of these devices. The IQE for the *t*-butyl SiNc absorption region seems to increase with concentration, reaching a maximum at about 60% in the highest concentration at a wavelength of 830 nm. Since the absorption is very low between the P3HT and *t*-butyl SiNc absorption bands, the reliability of the IQE values in these regions is poor. Still, the values near the absorption maxima are likely to be valid. The slight decrease in the IQE in the P3HT absorption region is likely due to a fraction of the excitons on P3HT transferring their energy to the *t*-butyl SiNc via a Forster resonance energy transfer mechanism (FRET)[61] and then splitting with the reduced efficiency associated with excitons

created on the *t*-butyl SiNc. The cause of the variation in the IQE with *t*-butyl SiNc concentration is beyond the scope of the work at this time.

To see the role of the *t*-butyl functionalization in determining improved performance, we prepared ternary blends of P3HT:$PC_{60}BM$ with the unfunctionalized SiNc and measured their performance. The devices with unfunctionalized SiNc were prepared in the same manner as the cells with *t*-butyl-functionalized SiNc and were also thermally annealed at 110 °C for 10 min. Figure 5a shows the *J*−*V* curves of several devices with increasing SiNc loading, showing a reduced benefit to solar cell performance. Table 2 summarizes these results. Figure 5b shows the EQE spectra of these devices with increasing SiNc loading. While the main absorption peak of SiNc at 800 nm is again evident in these devices, there is no appearance of a secondary peak at 830 nm in these devices, suggesting that the *t*-butyl functional group is important to the absorption shift.

To summarize, the J_{SC} of P3HT:$PC_{60}BM$ devices is significantly increased with the addition of *t*-butyl SiNc. The additional *t*-butyl group at the periphery of the SiNc molecule allows up to approximately 10 wt % of *t*-butyl SiNc to be incorporated before efficiency begins to plateau. The boost to the photocurrent is due to absorption of the dye in the 700−830 nm region, at an energy below the band gap of the P3HT but still above the energy of the charge transfer state, allowing charge transfer to occur via hole transfer to P3HT and electron transfer to $PC_{60}BM$. The *t*-butyl groups also play a role in the introduction of a red shift in the absorption at dye loadings greater than approximately 8 wt %. This absorption shift occurs only in ternary blend devices and not in either the P3HT:*t*-butyl SiNc or *t*-butyl SiNc:$PC_{60}BM$ devices, and only after a thermal annealing step. While it is not possible to conclusively determine the cause of this absorption shift, we believe that the higher concentration of dye forces the SiNc molecules to couple together, perhaps as a *J*-aggregate, or through covalent bond formation. This absorption shift allows a further broadening of the absorption bandwidth and additional increases to J_{SC}.

To further understand the role of the *t*-butyl functionalization in enabling higher dye loading in these films, we investigated the morphology of the ternary blends using two-dimensional wide-angle grazing incidence X-ray scattering (2-D GIWAXS) at the Stanford Synchrotron Radiation Lightsource (SSRL). Figure 6 shows X-ray scattering images for P3HT:$PC_{60}BM$ films, both as-cast and annealed (Figure 6a and 6b), along with images for ternary blends of P3HT:$PC_{60}BM$ with 20 wt % *t*-butyl SiNc (unannealed in Figure 6c and annealed in Figure 6d) and 20 wt % unfunctionalized SiNc (unannealed in Figure 6e and annealed in Figure 6f). The images of the ternary blend films (both as-cast and annealed) containing the *t*-butyl SiNc closely resemble the binary P3HT:$PC_{60}BM$ blend films, where the typical (100) and (010) peaks of the P3HT and characteristic ring of the $PC_{60}BM$ are clearly visible along with a few rings of moderate intensity that are likely due to scattering from the *t*-butyl SiNc molecules. This would be a scattering pattern that is commensurate with either a lightly disordered *t*-butyl SiNc phase or mixing of *t*-butyl SiNc molecules within a disordered P3HT, disordered $PC_{60}BM$, or mixed P3HT:$PC_{60}BM$ amorphous phase. In contrast, the ternary blends containing the unfunctionalized SiNc show significant scattering intensity from peaks not associated with either the P3HT or $PC_{60}BM$, indicating a highly ordered and textured SiNc phase within the ternary blend film. This pattern would be commensurate with a film morphology that has relatively large volumes of ordered SiNc phase and low fractions of SiNc molecules contained within an amorphous mixed phase between the P3HT and $PC_{60}BM$. These data, taken with the efficiency and EQE data, suggest that the morphological differences are the key reason behind the capability to incorporate higher volumes of *t*-butyl SiNc into the P3HT:$PC_{60}BM$ blend film without disruption of the optimal BHJ microstructure and resulting decrease in efficiency.

The relative energy levels of the P3HT, $PC_{60}BM$, and *t*-butyl SiNc dictate the likely mechanisms by which photocurrent can successfully be generated as well as provide information relating to the likely morphology of the ternary blend film. If the *t*-butyl SiNc molecules were wholly dispersed within the P3HT phase, they would likely act as electron traps where excitons generated in the P3HT could undergo electron transfer to the *t*-butyl SiNc (Figure 7a). This trapped electron could then recombine with free holes in the P3HT phase, resulting in current loss. An equivalent process would occur with the *t*-butyl SiNc molecules behaving as hole traps if the *t*-butyl SiNc were primarily dispersed within the $PC_{60}BM$ phase (Figure 7b). The most likely scenario for the location of the *t*-butyl SiNc that is commensurate with efficient photocurrent generation is for the *t*-butyl SiNc to be primarily located in the amorphous mixed P3HT:$PC_{60}BM$ region at the interface between the P3HT and $PC_{60}BM$ phases. Since photocurrent generation is efficient in these ternary blend systems, this is the most likely morphology for this ternary blend system. This conclusion was also reached using transient absorption spectroscopy by Honda et al. in the P3HT:$PC_{60}BM$:SiPc system.[61]

CONCLUSIONS

The functionalization of silicon naphthalocyanine molecules with *tert*-butyl groups on the periphery of the molecule results in significant changes to the morphological interaction between the dye molecules and the bulk heterojunction blend morphology in P3HT:$PC_{60}BM$ organic solar cells. With the *t*-butyl groups, the solubility limit of the SiNc dye in the P3HT:$PC_{60}BM$ system is higher than that of the unfunctionalized dye, allowing significantly more dye incorporation without disruption of the BHJ morphology or the formation of a highly ordered SiNc phase. This results in an increase in the spectral bandwidth of the absorption of the active layer and the maximum J_{SC} of the ternary blend film.

The *t*-butyl groups also enable the formation of an alternative morphological state of the SiNc molecule—perhaps in a dimeric state with two SiNc molecules directly adjacent to each other—that results in a red shift of the major SiNc absorption peak by 30 nm, expanding the spectral bandwidth of the ternary blend cell and ultimately resulting in an increase of 32% in J_{SC} and 19% in PCE.

ASSOCIATED CONTENT

Supporting Information

tert-Butyl silicon naphthalocyanine synthetic scheme, ^{1}H and ^{13}C NMR, MALDI spectrum, cyclic voltammetry traces, solution-state absorption spectra, and P3HT:*t*-butyl SiNc and *t*-butyl SiNc:$PC_{60}BM$ device absorption spectra. This material is available free of charge via the Internet at http://pubs.acs.org.

AUTHOR INFORMATION

Corresponding Author

*E-mail: aselli@mines.edu.

Present Address

[§]Corporate R&D, LG Chem. Research Park, 104-1 Moonji-dong, Yuseong-gu, Daejeon 305-380, South Korea.

Author Contributions

[‖]B.L. and J.T.B. contributed equally to this manuscript.

Notes

The authors declare no competing financial interest.

ACKNOWLEDGMENTS

This work was supported by the Office of Naval Research (ONR) through grant #N000141110244. The Bruker UltrafleXtreme MALDI/TOF-TOF mass spectrometer was purchased under the NSF-MRI grant #CHE-1229156.

REFERENCES

(1) Brabec, C. J.; Gowrisanker, S.; Halls, J. J.; Laird, D.; Jia, S.; Williams, S. P. Polymer-Fullerene Bulk-Heterojunction Solar Cells. *Adv. Mater.* **2010**, *22*, 3839−3856.

(2) Clarke, T. M.; Durrant, J. R. Charge Photogeneration in Organic Solar Cells. *Chem. Rev.* **2010**, *110*, 6736−6767.

(3) Darling, S. B.; You, F. The Case for Organic Photovoltaics. *RSC Adv.* **2013**, *3*, 17633−17648.

(4) Jørgensen, M.; Carlé, J. E.; Søndergaard, R. R.; Lauritzen, M.; Dagnæs-Hansen, N. A.; Byskov, S. L.; Andersen, T. R.; Larsen-Olsen, T. T.; Böttiger, A. P. L.; Andreasen, B.; Fu, L.; Zuo, L.; Liu, Y.; Bundgaard, E.; Zhan, X.; Chen, H.; Krebs, F. C. The State of Organic Solar Cells—a Meta Analysis. *Sol. Energy Mater. Sol. Cells* **2013**, *119*, 84−93.

(5) Li, G.; Zhu, R.; Yang, Y. Polymer Solar Cells. *Nat. Photonics* **2012**, *6*, 153−161.

(6) Yu, G.; Gao, J.; Hummelen, J. C.; Wudl, F.; Heeger, A. J. Polymer Photovoltaic Cells: Enhanced Efficiencies Via a Network of Internal Donor-Acceptor Heterojunctions. *Science* **1995**, *270*, 1789−1791.

(7) Dang, M. T.; Hirsch, L.; Wantz, G. P3HT:PCBM, Best Seller in Polymer Photovoltaic Research. *Adv. Mater.* **2011**, *23*, 3597−3602.

(8) Kim, Y.; Cook, S.; Tuladhar, S. M.; Choulis, S. A.; Nelson, J.; Durrant, J. R.; Bradley, D. D. C.; Giles, M.; McCulloch, I.; Ha, C. S.; Ree, M. A Strong Regioregularity Effect in Self-Organizing Conjugated Polymer Films and High-Efficiency Polythiophene: Fullerene Solar Cells. *Nat. Mater.* **2006**, *5*, 197−203.

(9) Li, G.; Shrotriya, V.; Huang, J. S.; Yao, Y.; Moriarty, T.; Emery, K.; Yang, Y. High-Efficiency Solution Processable Polymer Photovoltaic Cells by Self-Organization of Polymer Blends. *Nat. Mater.* **2005**, *4*, 864−868.

(10) Padinger, F.; Rittberger, R. S.; Sariciftci, N. S. Effects of Postproduction Treatment on Plastic Solar Cells. *Adv. Funct. Mater.* **2003**, *13*, 85−88.

(11) Schilinsky, P.; Waldauf, C.; Brabec, C. J. Recombination and Loss Analysis in Polythiophene Based Bulk Heterojunction Photodetectors. *Appl. Phys. Lett.* **2002**, *81*, 3885−3887.

(12) Campoy-Quiles, M.; Ferenczi, T.; Agostinelli, T.; Etchegoin, P. G.; Kim, Y.; Anthopoulos, T. D.; Stavrinou, P. N.; Bradley, D. D. C.; Nelson, J. Morphology Evolution Via Self-Organization and Lateral and Vertical Diffusion in Polymer:Fullerene Solar Cell Blends. *Nat. Mater.* **2008**, *7*, 158−164.

(13) Reyes-Reyes, M.; Kim, K.; Carroll, D. L. High-Efficiency Photovoltaic Devices Based on Annealed Poly(3-Hexylthiophene) and 1-(3-Methoxycarbonyl)-Propyl-1- Phenyl-(6,6)C[Sub 61] Blends. *Appl. Phys. Lett.* **2005**, *87*, 083506−083503.

(14) He, Y.; Chen, H.-Y.; Hou, J.; Li, Y. Indene−C60 Bisadduct: A New Acceptor for High-Performance Polymer Solar Cells. *J. Am. Chem. Soc.* **2010**, *132*, 1377−1382.

(15) He, Z.; Zhong, C.; Su, S.; Xu, M.; Wu, H.; Cao, Y. Enhanced Power-Conversion Efficiency in Polymer Solar Cells Using an Inverted Device Structure. *Nat. Photonics* **2012**, *6*, 591−595.

(16) Hoke, E. T.; Vandewal, K.; Bartelt, J. A.; Mateker, W. R.; Douglas, J. D.; Noriega, R.; Graham, K. R.; Fréchet, J. M. J.; Salleo, A.; McGehee, M. D. Recombination in Polymer:Fullerene Solar Cells with Open-Circuit Voltages Approaching and Exceeding 1.0 V. *Adv. Energy Mater.* **2013**, *3*, 220−230.

(17) Liang, Y.; Xu, Z.; Xia, J.; Tsai, S.-T.; Wu, Y.; Li, G.; Ray, C.; Yu, L. For the Bright Future-Bulk Heterojunction Polymer Solar Cells with Power Conversion Efficiency of 7.4%. *Adv. Mater.* **2010**, *22*, E135−E138.

(18) Park, S. H.; Roy, A.; Beaupre, S.; Cho, S.; Coates, N.; Moon, J. S.; Moses, D.; Leclerc, M.; Lee, K.; Heeger, A. J. Bulk Heterojunction Solar Cells with Internal Quantum Efficiency Approaching 100%. *Nat. Photonics* **2009**, *3*, 297−302.

(19) Piliego, C.; Holcombe, T. W.; Douglas, J. D.; Woo, C. H.; Beaujuge, P. M.; Frechet, J. M. J. Synthetic Control of Structural Order in N-Alkylthieno[3,4-C]Pyrrole-4,6-Dione-Based Polymers for Efficient Solar Cells. *J. Am. Chem. Soc.* **2010**, *132*, 7595−7597.

(20) Small, C. E.; Chen, S.; Subbiah, J.; Amb, C. M.; Tsang, S.-W.; Lai, T.-H.; Reynolds, J. R.; So, F. High-Efficiency Inverted Dithienogermole-Thienopyrrolodione-Based Polymer Solar Cells. *Nat. Photonics* **2012**, *6*, 115−120.

(21) Zhang, Y.; Hau, S. K.; Yip, H.-L.; Sun, Y.; Acton, O.; Jen, A. K. Y. Efficient Polymer Solar Cells Based on the Copolymers of Benzodithiophene and Thienopyrroledione. *Chem. Mater.* **2010**, *22*, 2696−2698.

(22) Zhao, G.; He, Y.; Li, Y. 6.5% Efficiency of Polymer Solar Cells Based on Poly(3-Hexylthiophene) and Indene-C(60) Bisadduct by Device Optimization. *Adv. Mater.* **2010**, *22*, 4355−4358.

(23) Zou, Y.; Najari, A.; Berrouard, P.; Beaupré, S.; Réda Aïch, B.; Tao, Y.; Leclerc, M. A Thieno[3,4-C]Pyrrole-4,6-Dione-Based Copolymer for Efficient Solar Cells. *J. Am. Chem. Soc.* **2010**, *132*, 5330−5331.

(24) Liao, S.-H.; Jhuo, H.-J.; Cheng, Y.-S.; Chen, S.-A. Fullerene Derivative-Doped Zinc Oxide Nanofilm as the Cathode of Inverted Polymer Solar Cells with Low-Bandgap Polymer (PTB7-Th) for High Performance. *Adv. Mater.* **2013**, *25*, 4766−4771.

(25) Chen, H. Y.; Hou, J. H.; Zhang, S. Q.; Liang, Y. Y.; Yang, G. W.; Yang, Y.; Yu, L. P.; Wu, Y.; Li, G. Polymer Solar Cells with Enhanced Open-Circuit Voltage and Efficiency. *Nat. Photonics* **2009**, *3*, 649−653.

(26) Chen, S.; Choudhury, K. R.; Subbiah, J.; Amb, C. M.; Reynolds, J. R.; So, F. Photo-Carrier Recombination in Polymer Solar Cells Based on P3HT and Silole-Based Copolymer. *Adv. Energy Mater.* **2011**, *1*, 963−969.

(27) Fei, Z.; Kim, J. S.; Smith, J.; Domingo, E. B.; Anthopoulos, T. D.; Stingelin, N.; Watkins, S. E.; Kim, J.-S.; Heeney, M. A Low Band Gap Co-Polymer of Dithienogermole and 2,1,3-Benzothiadiazole by Suzuki Polycondensation and Its Application in Transistor and Photovoltaic Cells. *J. Mater. Chem.* **2011**, *21*, 16257−16263.

(28) Hou, J.; Chen, H.-Y.; Zhang, S.; Li, G.; Yang, Y. Synthesis, Characterization, and Photovoltaic Properties of a Low Band Gap Polymer Based on Silole-Containing Polythiophenes and 2,1,3-Benzothiadiazole. *J. Am. Chem. Soc.* **2008**, *130*, 16144−16145.

(29) Bloking, J. T.; Han, X.; Higgs, A. T.; Kastrop, J. P.; Pandey, L.; Norton, J. E.; Risko, C.; Chen, C. E.; Brédas, J.-L.; McGehee, M. D.; Sellinger, A. Solution-Processed Organic Solar Cells with Power Conversion Efficiencies of 2.5% Using Benzothiadiazole/Imide-Based Acceptors. *Chem. Mater.* **2011**, *23*, 5484−5490.

(30) Chu, T.-Y.; Lu, J.; Beaupré, S.; Zhang, Y.; Pouliot, J.-R.; Wakim, S.; Zhou, J.; Leclerc, M.; Li, Z.; Ding, J.; Tao, Y. Bulk Heterojunction Solar Cells Using Thieno[3,4-C]Pyrrole-4,6-Dione and Dithieno[3,2-B:2′,3′-D]Silole Copolymer with a Power Conversion Efficiency of 7.3%. *J. Am. Chem. Soc.* **2011**, *133*, 4250−4253.

(31) Lenes, M.; Wetzelaer, G.-J. A. H.; Kooistra, F. B.; Veenstra, S. C.; Hummelen, J. C.; Blom, P. W. M. Fullerene Bisadducts for Enhanced Open-Circuit Voltages and Efficiencies in Polymer Solar Cells. *Adv. Mater.* **2008**, *20*, 2116−2119.

(32) Yuan, J.; Zhai, Z.; Dong, H.; Li, J.; Jiang, Z.; Li, Y.; Ma, W. Efficient Polymer Solar Cells with a High Open Circuit Voltage of 1 Volt. *Adv. Funct. Mater.* **2013**, *23*, 885−892.
(33) Nozawa, T. *Mitsubishi Chemical Claims Efficiency Record for Organic Thin-Film Pv Cell*. http://techon.nikkeibp.co.jp/english/NEWS_EN/20120601/221131/ (accessed May 6, 2013).
(34) Gupta, V.; Kyaw, A. K. K.; Wang, D. H.; Chand, S.; Bazan, G. C.; Heeger, A. J. Barium: An Efficient Cathode Layer for Bulk-Heterojunction Solar Cells. *Sci. Rep.* **2013**, *3*, 1965.
(35) Kyaw, A. K. K.; Wang, D. H.; Wynands, D.; Zhang, J.; Nguyen, T.-Q.; Bazan, G. C.; Heeger, A. J. Improved Light Harvesting and Improved Efficiency by Insertion of an Optical Spacer (Zno) in Solution-Processed Small-Molecule Solar Cells. *Nano Lett.* **2013**, *13*, 3796−3801.
(36) Ameri, T.; Khoram, P.; Min, J.; Brabec, C. J. Organic Ternary Solar Cells: A Review. *Adv. Mater.* **2013**, *25*, 4245−4266.
(37) Choi, J. W.; Kulshreshtha, C.; Kennedy, G. P.; Kwon, J. H.; Jung, S.-H.; Chae, M. Solution-Processed Bulk Heterojunction Organic Solar Cells with High Polarity Small Molecule Sensitizer. *Sol. Energy Mater. Sol. Cells* **2011**, *95*, 2069−2076.
(38) Hesse, H. C.; Weickert, J.; Hundschell, C.; Feng, X.; Müllen, K.; Nickel, B.; Mozer, A. J.; Schmidt-Mende, L. Perylene Sensitization of Fullerenes for Improved Performance in Organic Photovoltaics. *Adv. Energy Mater.* **2011**, *1*, 861−869.
(39) Honda, S.; Nogami, T.; Ohkita, H.; Benten, H.; Ito, S. Improvement of the Light-Harvesting Efficiency in Polymer/Fullerene Bulk Heterojunction Solar Cells by Interfacial Dye Modification. *ACS Appl. Mater. Interfaces* **2009**, *1*, 804−810.
(40) Huang, J.-H.; Velusamy, M.; Ho, K.-C.; Lin, J.-T.; Chu, C.-W. A Ternary Cascade Structure Enhances the Efficiency of Polymer Solar Cells. *J. Mater. Chem.* **2010**, *20*, 2820−2825.
(41) Kubo, Y.; Watanabe, K.; Nishiyabu, R.; Hata, R.; Murakami, A.; Shoda, T.; Ota, H. Near-Infrared Absorbing Boron-Dibenzopyrromethenes That Serve as Light-Harvesting Sensitizers for Polymeric Solar Cells. *Org. Lett.* **2011**, *13*, 4574−4577.
(42) Sharma, S. S.; Sharma, G. D.; Mikroyannidis, J. A. Improved Power Conversion Efficiency of Bulk Heterojunction Poly(3-Hexylthiophene):PCBM Photovoltaic Devices Using Small Molecule Additive. *Sol. Energy Mater. Sol. Cells* **2011**, *95*, 1219−1223.
(43) Umeda, T.; Hashimoto, Y.; Mizukami, H.; Noda, H.; Fujii, A.; Ozaki, M.; Yoshino, K. Improvement of Sensitivity in Long-Wavelength Range in Organic Thin-Film Solar Cell with Interpenetrating Semilayered Structure. *Jpn. J. Appl. Phys.* **2006**, *45*, 538.
(44) Ameri, T.; Heumuller, T.; Min, J.; Li, N.; Matt, G.; Scherf, U.; Brabec, C. J. Ir Sensitization of an Indene-C60 Bisadduct (ICBA) in Ternary Organic Solar Cells. *Energy Environ. Sci.* **2013**, *6*, 1796−1801.
(45) Ameri, T.; Min, J.; Li, N.; Machui, F.; Baran, D.; Forster, M.; Schottler, K. J.; Dolfen, D.; Scherf, U.; Brabec, C. J. Performance Enhancement of the P3HT/PCBM Solar Cells through Nir Sensitization Using a Small-Bandgap Polymer. *Adv. Energy Mater.* **2012**, *2*, 1198−1202.
(46) Chen, M. C.; Liaw, D. J.; Huang, Y. C.; Wu, H. Y.; Tai, Y. Improving the Efficiency of Organic Solar Cell with a Novel Ambipolar Polymer to Form Ternary Cascade Structure. *Sol. Energy Mater. Sol. Cells* **2011**, *95*, 2621−2627.
(47) Kim, H.; Shin, M.; Kim, Y. Distinct Annealing Temperature in Polymer:Fullerene:Polymer Ternary Blend Solar Cells. *J. Phys. Chem. C* **2009**, *113*, 1620−1623.
(48) Koppe, M.; Egelhaaf, H.-J.; Dennler, G.; Scharber, M. C.; Brabec, C. J.; Schilinsky, P.; Hoth, C. N. Near Ir Sensitization of Organic Bulk Heterojunction Solar Cells: Towards Optimization of the Spectral Response of Organic Solar Cells. *Adv. Funct. Mater.* **2010**, *20*, 338−346.
(49) Lobez, J. M.; Andrew, T. L.; Bulović, V.; Swager, T. M. Improving the Performance of P3HT−Fullerene Solar Cells with Side-Chain-Functionalized Poly(Thiophene) Additives: A New Paradigm for Polymer Design. *ACS Nano* **2012**, *6*, 3044−3056.
(50) Huang, J.-S.; Goh, T.; Li, X.; Sfeir, M. Y.; Bielinski, E. A.; Tomasulo, S.; Lee, M. L.; Hazari, N.; Taylor, A. D. Polymer Bulk Heterojunction Solar Cells Employing Forster Resonance Energy Transfer. *Nat. Photonics* **2013**, *7*, 479−485.
(51) Sharma, G. D.; Singh, S. P.; Roy, M. S.; Mikroyannidis, J. A. Solution Processed Bulk Heterojunction Polymer Solar Cells with Low Band Gap DPP-CN Small Molecule Sensitizer. *Org. Electron.* **2012**, *13*, 1756−1762.
(52) Xu, Z.-X.; Roy, V. A. L.; Low, K.-H.; Che, C.-M. Bulk Heterojunction Photovoltaic Cells Based on Tetra-Methyl Substituted Copper(II) Phthalocyanine:P3HT:PCBM Composite. *Chem. Commun.* **2011**, *47*, 9654−9656.
(53) Yang, L.; Zhou, H.; Price, S. C.; You, W. Parallel-Like Bulk Heterojunction Polymer Solar Cells. *J. Am. Chem. Soc.* **2012**, *134*, 5432−5435.
(54) Khlyabich, P. P.; Burkhart, B.; Thompson, B. C. Compositional Dependence of the Open-Circuit Voltage in Ternary Blend Bulk Heterojunction Solar Cells Based on Two Donor Polymers. *J. Am. Chem. Soc.* **2012**, *134*, 9074−9077.
(55) Kang, H.; Kim, K.-H.; Kang, T. E.; Cho, C.-H.; Park, S.; Yoon, S. C.; Kim, B. J. Effect of Fullerene Tris-Adducts on the Photovoltaic Performance of P3HT:Fullerene Ternary Blends. *ACS Appl. Mater. Interfaces* **2013**, *5*, 4401−4408.
(56) Khlyabich, P. P.; Burkhart, B.; Thompson, B. C. Efficient Ternary Blend Bulk Heterojunction Solar Cells with Tunable Open-Circuit Voltage. *J. Am. Chem. Soc.* **2011**, *133*, 14534−14537.
(57) Li, H.; Zhang, Z.-G.; Li, Y.; Wang, J. Tunable Open-Circuit Voltage in Ternary Organic Solar Cells. *Appl. Phys. Lett.* **2012**, *101*, 163302−163305.
(58) Street, R. A.; Davies, D.; Khlyabich, P. P.; Burkhart, B.; Thompson, B. C. Origin of the Tunable Open-Circuit Voltage in Ternary Blend Bulk Heterojunction Organic Solar Cells. *J. Am. Chem. Soc.* **2013**, *135*, 986−989.
(59) Honda, S.; Ohkita, H.; Benten, H.; Ito, S. Multi-Colored Dye Sensitization of Polymer/Fullerene Bulk Heterojunction Solar Cells. *Chem. Commun.* **2010**, *46*, 6596−6598.
(60) Honda, S.; Ohkita, H.; Benten, H.; Ito, S. Selective Dye Loading at the Heterojunction in Polymer/Fullerene Solar Cells. *Adv. Energy Mater.* **2011**, *1*, 588−598.
(61) Honda, S.; Yokoya, S.; Ohkita, H.; Benten, H.; Ito, S. Light-Harvesting Mechanism in Polymer/Fullerene/Dye Ternary Blends Studied by Transient Absorption Spectroscopy. *J. Phys. Chem. C* **2011**, *115*, 11306−11317.
(62) Plater, M. J.; Jeremiah, A.; Bourhill, G. Synthesis of Soluble Halogenated Aryloxy Substituted Indium Phthalocyanines. *J. Chem. Soc., Perkin Trans. 1* **2002**, *0*, 91−96.
(63) Lim, B.; Margulis, G. Y.; Yum, J.-H.; Unger, E. L.; Hardin, B. E.; Grätzel, M.; McGehee, M. D.; Sellinger, A. Silicon-Naphthalo/Phthalocyanine-Hybrid Sensitizer for Efficient Red Response in Dye-Sensitized Solar Cells. *Org. Lett.* **2013**, *15*, 784−787.
(64) Bartelmess, J.; Soares, A. R. M.; Martinez-Diaz, M. V.; Neves, M. G. P. M. S.; Tome, A. C.; Cavaleiro, J. A. S.; Torres, T.; Guldi, D. M. Panchromatic Light Harvesting in Single Wall Carbon Nanotube Hybrids-Immobilization of Porphyrin-Phthalocyanine Conjugates. *Chem. Commun.* **2011**, *47*, 3490−3492.
(65) Burkhard, G. F.; Hoke, E. T.; McGehee, M. D. Accounting for Interference, Scattering, and Electrode Absorption to Make Accurate Internal Quantum Efficiency Measurements in Organic and Other Thin Solar Cells. *Adv. Mater.* **2010**, *22*, 3293−3297.